Blackbody Infrared Radiative Dissociation of Partially Solvated Tris(2,2′-bipyridine)ruthenium(II) Complex Ions†

Stanley M. Stevens Jr.,‡ Robert C. Dunbar,§ William D. Price,|| Marcelo Sena,⊥ Clifford H. Watson,‡,# Linda S. Nichols,‡,$ Jose M. Riveros,⊥ David E. Richardson,‡ and John R. Eyler*,‡

Department of Chemistry, P.O. Box 117200, University of Florida, Gainesville, Florida 32611-7200, Chemistry Department, Case Western Reserve University, Cleveland, Ohio 44106, Department of Chemistry, Marshall University, Huntington, West Virginia 25755, and Instituto de Química, Universidade de São Paulo, São Paulo-SP, Brazil, Caixa Postal 26077, CEP 05599-970

Received: March 29, 2002; In Final Form: July 22, 2002

Electrospray ionization Fourier transform ion cyclotron resonance (ESI-FTICR) mass spectrometry has been utilized to study solvates of tris(2,2′-bipyridine)ruthenium(II). Spontaneous dissociation of solvent (acetonitrile, acetone, or methyl ethyl ketone) from the solvation shell occurs when these ions are trapped for extended periods of time in the ICR cell. The pressures employed in these experiments are low enough (10^{-9} to 10^{-8} mbar) to neglect (or partially neglect) collisional activation as a means for dissociation. Therefore, it is suggested that the solvated ruthenium species undergo dissociation following the absorption of blackbody infrared radiation. Solvent−complex dissociation has been studied at several pressures ranging from 10^{-9} to 10^{-8} mbar to provide a range of dissociation data in the low-pressure regime. The results reported here demonstrate the consistency of the dissociation rate constants at pressures that differ by an order of magnitude. Temperature dependence studies were performed to extract zero-pressure activation energies from Arrhenius analyses. Given the number of degrees of freedom and the magnitude of the rate constants at a given temperature of the ruthenium complex ion solvates, the experimental Arrhenius activation energies are likely to be substantially lower than the true bond dissociation energies. ZINDO semiempirical methods, which were calibrated against DFT and experimental values, have been used to determine optimized structures and vibrational frequencies for bipyridine-containing ruthenium(II) solvates. These parameters were then used both for master equation modeling and the truncated Boltzmann/modified Tolman approach, each of which provide calculated binding energies of the solvents to the ruthenium complex ion. Solvation energies in the range 15−20 kcal/mol were found for binding of solvent molecules in the first solvation shell of tris(2,2′-bipyridine) ruthenium(II) ions.

Introduction

Polypyridine complexes of divalent ruthenium ions have been of major interest for applications such as analytical chemiluminescence[1] and solar energy conversion.[2] The prototype complex of this group is tris(2,2′-bipyridine)ruthenium(II), $[Ru(bpy)_3]^{2+}$ (Figure 1), and a vast number of derivatives have also been studied.[3] Extensive work has been done by Woodruff[4] and Kincaid[5] on normal-coordinate analysis of both the ground and MLCT excited states of tris(bipyridine)ruthenium(II). The possible use of these compounds in solar energy conversion as well as investigation of their unique excited-state properties[6,7] has pointed out the need for even better understanding of their structure and reactivity.

Fourier transform ion cyclotron resonance (FT-ICR) mass spectrometry[8,9] has proven to be a powerful tool for studying gas-phase ion chemistry. FT-ICR mass spectrometry offers high mass accuracy,[10] nondestructive detection (remeasurement of the same ion population for improved sensitivity, high orders of multistage mass spectrometry, etc.),[11] and unparalleled mass resolving power.[12] Additionally, due to the long trapping times obtainable by FT-ICR methodology, a variety of experimental techniques can be employed to manipulate the ions trapped in the ICR cell. After formation by electrospray ionization (ESI),[13,14] noncovalent complexes, such as the solvated ruthenium clusters used in these experiments, can be transferred to the FT-ICR analyzer cell and investigated in the gas phase. Analysis of these partially solvated gas-phase ions provides a better understanding of the similarities and differences between solution and gas-phase chemistry by providing a bridge between the properties of the unsolvated ion in the gas phase and the same species in solution. The stepwise solvation energies of coordination complexes such as $[Ru(bpy)_3]^{2+}$ are fundamental physical properties that can reveal details about environmental effects in the excited-state chemistry of the ions.

Blackbody infrared radiative dissociation (BIRD) has been used as a reliable means to obtain unimolecular dissociation rate constants and dissociation energies for a variety of small to large molecular species.[15−26] Depending on several factors, including transition state structure, dissociation rate, magnitude

† Part of the special issue "Jack Beauchamp Festschrift".
* Corresponding author.
‡ University of Florida.
§ Case Western Reserve University.
|| Marshall University.
⊥ Universidade de São Paulo.
Current Address: Centers for Disease Control and Prevention, Air Toxicants Branch, Atlanta, GA 30341-3724.
$ Current Address: Savannah River Technology Center, Westinghouse Savannah River Co., Aiken, SC 29808.

10.1021/jp025860b CCC: $22.00
Published on Web 09/06/2002

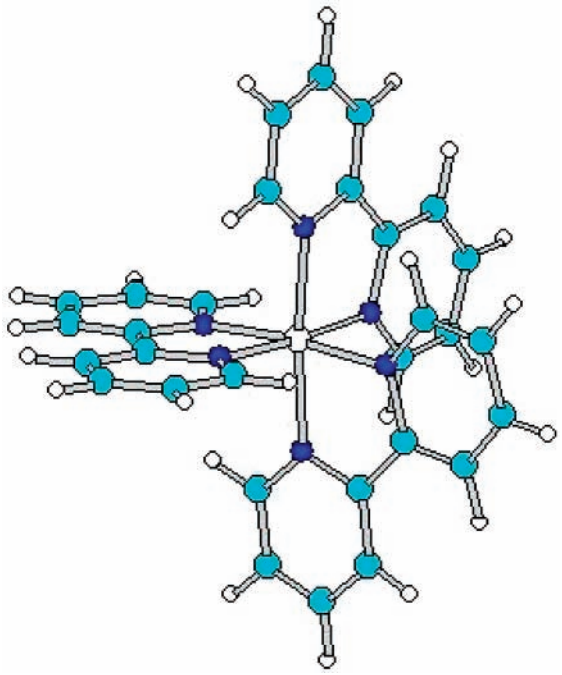

Figure 1. Cartoon structure of tris(2,2′-bipyridine)ruthenium(II). The nitrogens (dark atoms) are coordinatively bound to the central ruthenium ion to form an octahedral complex.

of activation energy, and the number of vibrational degrees of freedom, detailed calculations may or may not be required to extract the dissociation energies that govern BIRD processes.[27−29] For the solvated ruthenium complex ions studied here, a full master equation (ME)[30−32] approach has been utilized to determine desolvation energies associated with the solvent−complex bond. These results have also been compared with binding energies obtained from the truncated Boltzmann/modified Tolman approach.[27]

Experimental Section

All experiments were performed on a Bruker (Billerica, MA) FT-ICR mass spectrometer (BioApex 4.7e), which is equipped with a 4.7 T passively shielded superconducting magnet and coupled to a modified (heated metal capillary) Analytica (Branford, CT) ESI source.[33] Solutions containing the ruthenium complex ion were electrosprayed (V_{needle} = 1800 V) at a concentration of 2×10^{-5} M in methanol using a flow rate of 1.0 μL/min. The desolvating metal capillary was maintained at a voltage of 72 V and resistively heated to a temperature of 110 °C. The skimmer voltage was held at 5 V to generate a ΔV between the capillary and skimmer of 67 V. Capillary and skimmer voltages were minimized to reduce the chance of in-source dissociation processes. Resolvation of Ru(II) complex ions occurred after introduction of solvent-saturated nitrogen gas, which had been bubbled through the solvent of interest, into the electrospray source housing (Figure 2). This solvation method was first demonstrated by Posey et al.[34] A variety of partially solvated Ru(II) complex ions has been produced in our laboratory with this method using methanol, acetonitrile, acetone, and methyl ethyl ketone (MEK) as solvents.

Solvated ions were externally accumulated in a hexapole ion guide/trap for 1 s and subsequently transferred to the ICR cell via a series of electrostatic optics. The reaction delay time (before ion excitation and detection but after ion injection into the FTICR analyzer cell and any necessary ion ejections) was varied within the experimental pulse sequence to observe the

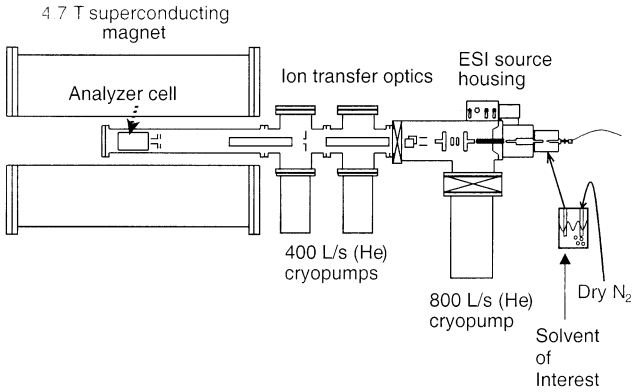

Figure 2. Schematic diagram of the FTICR mass spectrometer used in the BIRD experiments. House nitrogen was dried and bubbled through the solvent of interest. The "carrier" gas was then introduced into the ESI source housing where resolvation occurred after the capillary exit.

degree of blackbody infrared dissociation that occurred while the solvated species were trapped in the cell. Ion ejection/isolation experiments were performed by introducing a correlated sweep[35] into the pulse sequence, which inherently minimizes off-resonance excitation. In addition, a 10 kHz "safety belt" was applied on either side of the isolated ion frequency region to minimize energy imparted to the ion by frequencies of the chirp excitation nearest to that of the ion of interest.

Reasonable signal-to-noise was achieved upon mass spectral averaging of only a few scans. In general, however, 20−30 time domain signals were co-added prior to Fourier transformation to improve the quality of mass spectra and also to obtain a more accurate representation of relative ion populations in the ICR analyzer cell.

After isolation of a particular solvated ion, its peak height was monitored as a function of the reaction delay time to obtain an experimental unimolecular dissociation rate constant. Rate constants were obtained by plotting $\ln\{[M]/([M] + [P])\}$ versus reaction delay time, where M is the height of the solvated molecular ion peak and P is that of the dissociation product ion. This analysis method was more straightforward than fitting many peak heights as a function of reaction time because contributions from ions resulting from competing dissociation pathways involving other solvated species were minimized.

Pressure dependence studies were carried out by introducing argon directly into the FTICR cell via a Varian (Lexington, MA, Model 951-5106) leak valve with pressures ranging from 2×10^{-9} mbar (base pressure) to 5×10^{-8} mbar. Accurate BIRD kinetic modeling could not be accomplished at pressures greater than 10^{-7} mbar because activation by collisions contributes significantly to the dissociation mechanism. Moreover, substantial collisional damping of the ion signal occurs above 10^{-7} mbar, which in turn prevents meaningful evaluation of kinetic data above the defined low-pressure regime.

Temperature dependence studies were performed by directly heating the vacuum chamber around the analyzer cell. FTICR cell temperatures were elevated by controlling the power output of the bakeout heaters surrounding the vacuum chamber (in the region of the cell) via a Eurotherm [Reston, VA, Model 818] temperature controller. Temperatures in the analyzer cell were measured by two copper−constantan thermocouples, one attached to each of the electrically insulated structures that support the two opposing trapping plates. The average of the temperatures indicated by the two thermocouples was taken as the cell temperature. Calibration was accomplished with a third ther-

TABLE 1: Representative Vibrational Frequencies (cm^{-1}) Obtained from ZINDO for $[Ru(bpy)_3]^{2+}$ [a]

vibrational frequency	scaled vibrational frequency	experimental frequency[b]
166	182	207
233	250	283
447	455	370
712	681	668
1218	1048	1115
1400	1165	1176
2117	1571	1450
4788	2965	3071

[a] Scaling of the calculated frequencies to values closer to those observed experimentally was accomplished using eq 1. [b] Taken from ref 53.

mocouple placed directly in the center of the cell (only during calibration experiments). The average temperature from the two thermocouples at either end of the cell was always found to be within ±3 K of the third thermocouple reading over a temperature range of 294−365 K.

Computational Section

Zerner intermediate neglect of differential overlap (ZINDO)[36,37] (Hyperchem program v.5.1, Hypercube Inc., Gainesville, FL) semiempirical calculations and ME modeling were employed to determine binding energies for the solvent molecules attached to the Ru(II) complex ion. ZINDO has often been used to compute the properties of large molecular complexes containing transition metals.[38,39] All geometries of solvated Ru(II) complex ions were optimized using this semiempirical technique. Additionally, vibrational spectra were calculated to obtain vibrational frequencies and intensities required for ME modeling. Because ZINDO-calculated vibrations for C−H stretching modes differ greatly from average experimental values, a scaling formula of the form

$$\nu_{\text{scaled}} = \nu_i \sqrt{\left\{0.89 + \left[0.745 \sin\left(\frac{\pi}{2}\frac{(\nu_i - \nu_{\min})}{(\nu_{\max} - \nu_{\min})}\right)\right]\right\}} \quad (1)$$

was used (Zerner, private communication), where ν_i is the ZINDO-calculated frequency of interest, and $\nu_{\min}$ and $\nu_{\max}$ are the lowest and highest ZINDO-calculated frequencies, respectively. Table 1 shows some selected vibrational frequencies obtained from the ZINDO method for tris(2,2′-bipyridine)-ruthenium(II) solvated with one MEK molecule, the corresponding scaled frequencies, and experimental frequencies. Low frequencies are scaled to slightly higher values, whereas those at ∼4500 cm^{-1}, associated with C−H stretching frequencies, are scaled to experimentally observed values around 3000 cm^{-1}.

ZINDO-optimized geometries of $[Ru(bpy)_3]^{2+}$ and the solvent molecule acetonitrile were used as input for density functional theory, DFT, calculations at the B3LYP/LANL2DZ level of theory using the Gaussian 98[40] computational package. DFT optimized structures were then used for the calculation of vibrational frequencies and absolute absorption intensities. The LANL2DZ basis set uses an effective core potential developed by Hay and Wadt[41−43] (Los Alamos National Laboratories) plus the DZ basis set to describe the elements Na to Bi. The Dunning/Huzinaga full double-ζ (D95)[44] basis set was used for the first row elements. DFT vibrational frequencies scaled by 0.95 gave the best agreement with experimental values as well as the scaled ZINDO frequency values.

Scaled vibrational frequencies obtained from ZINDO calculations were also used for truncated Boltzmann analysis. Densities of states required for the determination of Boltzmann statistics were calculated by using the Beyer−Swinehart direct count method.[45] A modified Tolman equation developed by Dunbar[27] was utilized

$$E_t = E_a + \langle E' \rangle - \Delta E_{\text{dep}} - \Delta E_{\text{rad}} \quad (2)$$

where ΔE_{dep} is the correction for the reactive depletion of the Boltzmann distribution and ΔE_{rad} consists of the blackbody radiation-related corrections. The sum of the partially canceling terms $\Delta E_{\text{dep}} + \Delta E_{\text{rad}}$ is estimated to be 300 cm^{-1}.[27]

Two master equation modeling programs, at Marshall University and at Case Western Reserve University (CWRU), were used, which are similar in concept but differ in some computational details and in some assumptions incorporated into the modeling. The comparison of results from these two independent analyses serves to suggest the magnitude of the uncertainty that is associated with differing assumptions and choices made in fitting the data to a kinetic-theory model.

Briefly, the master equation model numerically simulates the experiment as the solution to a set of coupled integro-differential equations explicitly accounting for the detailed rates of all state-to-state transitions (k_{ij}) and dissociation processes (k_d). The coupled equations of motion are given by

$$dN_i(t) = [k_d N_i(0) + \sum_j k_{ij} N_j(0)]\, dt \quad (3)$$

where $N_j(0)$, $N_i(0)$, and $dN_i(t)$ are the initial population fraction in energy levels j and i and the time dependent change in population fraction in energy level i, respectively. The microcanonical dissociation rates (k_d) are determined either from RRKM theory or phase space theory using the reactant and transition state frequency sets described above. The sum and density of states were calculated using the direct count Beyer−Swinehart algorithm with an energy grain size of 1 cm^{-1}. In the zero-pressure limit, the rates of state-to-state transitions are given exclusively by the rates of radiative absorption ($k_{1,\text{rad}}$) and emission ($k_{-1,\text{rad}}$).

$$k_{i,j} = k_{1,\text{rad}} + k_{-1,\text{rad}} \quad (4)$$

The detailed rate constants for blackbody absorption, $k_{1,\text{rad}}$, and for spontaneous and stimulated emission, $k_{-1,\text{rad}}$, were calculated using the weakly coupled harmonic oscillator model.

$$k_{1,\text{rad}}(\Delta E_{i\to j} = h\nu) = \sum_m \rho(h\nu)\, \mathbf{B}(h\nu) P_i^{mh\nu} \quad (5)$$

$$k_{-1,\text{rad}}(\Delta E_{j\to i} = h\nu) = \sum_m \{\mathbf{A}(h\nu) + \rho(h\nu)\, \mathbf{B}(h\nu)\} P_j^{mh\nu} \quad (6)$$

where $P_j^{mh\nu}$ is the product of the probability of the νth oscillator having m quanta of energy in the jth internal energy state and of the increased transition probability of an excited harmonic oscillator, $\rho(h\nu)$ is the radiation density at ν given by the Planck distribution, and $\mathbf{B}(h\nu)$ and $\mathbf{A}(h\nu)$ are the Einstein coefficients for stimulated and spontaneous radiative transition processes, respectively, given by

$$\mathbf{B}(h\nu) = \mu^2 / 6\epsilon_0 \hbar^2 \quad (7)$$

$$\mathbf{A}(h\nu) = 8\pi h(\nu/c)^3 \mathbf{B}(h\nu) \quad (8)$$

As discussed above, transition frequencies (ν) calculated at the ZINDO *semiempirical* level were scaled using eq 1 and DFT frequencies were scaled by 0.95.

Master equation modeling at Marshall University was performed using double precision Fortran 77 code on a DEC 433AU workstation. A finite-difference approximation to the master equation, with an energy grain size of 50 cm^{-1}, was used to model the dissociation of these solvated complexes. Integration of stiffly coupled equations was facilitated by library calls to a freeware backward differentiation formula (BDF) routine (DVODE) provided within the ODEPACK library.[46] A Boltzmann distribution at each simulation temperature was used for the initial population. After a steady-state population distribution was reached, data points at a minimum of 12 "reaction" times were collected to evaluate the unimolecular rate constant. This process was repeated for each complex at two or three temperatures spanning the experimental temperature range. Arrhenius constants were obtained from the temperature dependence of these rate constants.

Within the RRKM/master equation model three parameters can be varied to fit the experimental Arrhenius constants: the threshold dissociation energy (E_0), the oscillator transition dipole moments (μ), and the transition frequency set associated with the activation entropy ($\Delta S^{\ddagger}$). Transition frequency sets were obtained from frequency analysis of the DFT or ZINDO calculations. The vibrational frequency corresponding to the dissociation reaction coordinate was removed from the set and five other low-frequency vibrations associated with coupling motion were systematically varied to generate activation entropies ranging from 0 to 15 eu. Four transition frequency sets were constructed for each system. The quality of transition dipole moments obtained from *semiempirical* and DFT theoretical models is not well characterized. For these calculations, scaling factors from 0.8 to 1.5 were used. It was not possible to fit the experimental data by scaling above or below this range.

The master equation modeled threshold dissociation energies reported here are obtained by systematically varying all three of these parameters over the stated ranges and comparing the resulting activation parameters with the experimental values. Calculated values within the error range of the experimental values are considered acceptable. Typically, only a few E_0 values are accepted within these constraints and the reported values include the full range.

In the CWRU contribution to the interpretation the master equation analysis was carried out both using an RRKM approach parallel to the Marshall University work, and also using a phase space theory (PST) approach. In all of this work, the master equation was analyzed with the matrix approach,[32] as implemented in the kinetics package VariFlex.[47] In this approach, the master eq 3 is put into matrix form, and the matrix is diagonalized. The lowest eigenvalue gives the steady-state rate constant for ion dissociation, and the corresponding eigenvector gives the steady-state internal-energy distribution of the ion population.

The microcanonical unimolecular dissociation rate constants for eq 3 were derived within the overall context of transition state theory (TST), using either RRKM theory or phase space theory (PST). A major uncertainty in the analysis is the nature of the transition state appropriate to these dissociations, which has a substantial effect on the results. Nearly all of the ions were calculated by both of these approaches.

The PST transition state adopts the limit of a very loose ("orbiting") transition state, which offers no empirical parametrization of the transition state. This is the loosest possible transition state within TST, and it gives low dissociation rates (or, equivalently, high dissociation energies) compared with models using a tighter transition state, which includes most RRKM parametrizations.

RRKM theory, when applied to barrierless dissociations (which is presumably the situation for the present solvent detachment reactions) uses a parametrized transition state, where the looseness of the transition state is parametrized in the form of an entropy of activation. This is carried out by a rather arbitrary procedure of adjusting the frequencies of various vibrational modes in the transition state. This entropy of activation is often specified at 1000 K and designated $\Delta S^{\ddagger}_{1000K}$. To a good degree of approximation, the two fitting parameters of the RRKM data fitting approach, namely, E_0 and $\Delta S^{\ddagger}_{1000K}$, trade off in such a way that very similar calculated kinetics result from pairs of matching E_0 and $\Delta S^{\ddagger}_{1000K}$ values over quite a wide range. A tight transition state (low $\Delta S^{\ddagger}_{1000K}$) combined with a low E_0 gives results similar to a loose transition state (highly positive $\Delta S^{\ddagger}_{1000K}$) combined with a high E_0. It was found in the present systems that a $\Delta S^{\ddagger}_{1000K}$ of 12−16 cal K^{-1} mol^{-1} gave results similar to the PST results (using the same E_0 values). However, this is a looser transition state than has usually been adopted in RRKM calculations[48] (also compare the Marshall University parametrization in the present work, described above), and it seemed best to use a somewhat lower value. In these calculations, $\Delta S^{\ddagger}_{1000K}$ was chosen near 10 cal K^{-1} mol^{-1}. This results in the RRKM assignments of E_0 being roughly 2 kcal/mol lower than the PST assignments, but it should be reemphasized that the RRKM assignments of absolute E_0 values depend fundamentally on the value chosen for $\Delta S^{\ddagger}_{1000K}$.

Most of the PST calculations used harmonic vibrational frequencies and transition dipole moments computed using a semiempirical "ZINDO" protocol. This involved ZINDO calculation of the harmonic frequencies and radiative intensities of the complex ion, followed by an empirical adjustment procedure designed to bring the important low-frequency modes into agreement with results of ab initio calculations. A few comparative PST calculations were also carried out using harmonic frequencies and intensities directly calculated by the density functional theory (DFT) approach using the B3LYP hybrid functional. Comparisons using both approaches to vibrational calculations gave similar results, and the much less computationally demanding ZINDO-based protocol was adopted for most systems. In all cases, a set of the lowest-frequency vibrational modes of the complex (one per solvent molecule) were identified as nearly free rotations of the solvent molecule around the binding axis. These modes were replaced in the calculations by internal free rotors with appropriate moments of inertia. In the RRKM calculations the solvent molecule being detached was assigned two additional free rotations in the transition state. (In the PST transition state the detaching molecule is intrinsically assumed to be freely rotating.)

The observed dissociation kinetics reflect the value of E_0 both in the absolute dissociation rates and in the slope of the temperature dependence. Ideally, analysis of these two types of data would give the same value of E_0, but in most of the present cases the absolute rates fitted a lower value of E_0 than the slopes, the difference being of the order of 2−3 kcal/mol. It seems best to rely most heavily on the slopes. The argument for this is that modeling the absolute dissociation rates is directly affected by the uncertainty of the photon absorption rate, whereas the slope is relatively insensitive to this aspect of the modeling. This is a particularly uncertain aspect of the modeling,

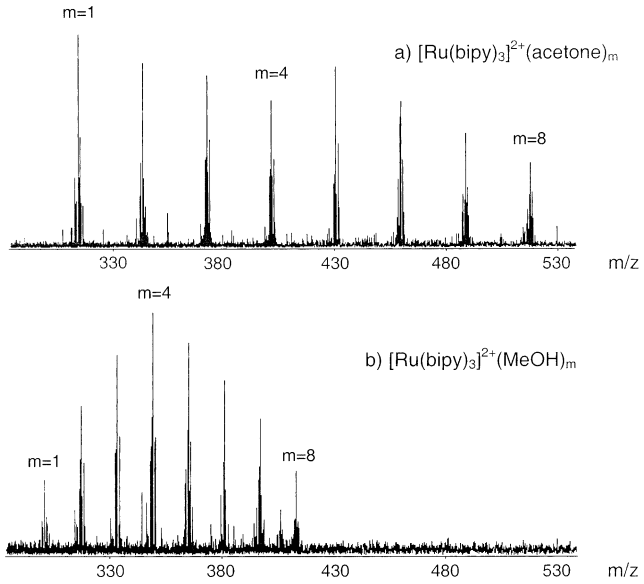

Figure 3. FTICR mass spectra of tris(2,2′-bipyridine)ruthenium(II) solvated with (a) acetone and (b) methanol molecules ($m = 1-8$). Species of m/z greater than $m = 8$ and less than $m = 1$ were ejected from the analyzer cell prior to detection.

because accurate calculation of the infrared radiative intensities is difficult even at a high level of computation. Calculated absolute dissociation rate predictions might easily be wrong by a factor of 2 on this account, even without considering the additional uncertainties discussed above in the TST modeling of the unimolecular dissociation rate constants. Therefore, the E_0 values reported from CWRU calculations are based on fitting the slopes.

Once the choice has been made of which transition state model to use, and the vibrational frequencies and intensities and other molecular properties have been assigned, the process of fitting an E_0 value to the observed temperature dependence is quite well constrained. The fitting uncertainty was of the order of ± 1 kcal/mol.

Results and Discussion

Solvated $[Ru(bpy)_3]^{2+}$ ions have been successfully generated and transferred to the ICR analyzer cell in our laboratory with a variety of solvent molecules still attached. The most critical factors influencing the solvation of these ruthenium complex ions were the capillary temperature and flow rate of the solvent-carrier gas into the ESI source housing. Other important parameters included the ion transfer orifice diameter of the heated capillary and pressure in the capillary-skimmer region. FT-ICR mass spectra of the $[Ru(bpy)_3]^{2+}$ ion with partial solvation by acetone and methanol solvents are shown in Figure 3a,b, respectively. The groups of peaks for each solvated ion shown in these mass spectra arise from the several isotopes of ruthenium as well as contributions from ^{13}C and ^{15}N. The extent of clustering varies with solvent due to steric effects, charge interactions, and other chemical influences. In general, the peak height of the most abundant solvated ion was between 30 and 50% that of the unsolvated molecular ion. Additionally, no "magic number" was apparent for the number of solvents attached to $[Ru(bpy)_3]^{2+}$; however, the ion peak heights typically decreased as a function of the number of solvent molecules attached to the ruthenium complex ion. As many as 18 MEK solvent molecules attached to $[Ru(bpy)_3]^{2+}$ have been observed, as well as H_2O/CH_3OH clusters of $[Ru(bpy)_3]^{2+}$ at higher m/z values. Following isolation of a Ru(II) complex ion with a specific number of solvent molecules attached (as described in the Experimental Section), loss of one solvent molecule was followed as a function of time. Figure 4 shows plots of the loss of one MEK solvent molecule from $[Ru(bpy)_3]^{2+}(MEK)_m$ ($m = 1-4$) as a function of trapping time in the FT-ICR cell at 329 K and a pressure of 3×10^{-9} mbar. The dissociation rate constant increases with the increasing degree of solvation around the ruthenium complex ion.

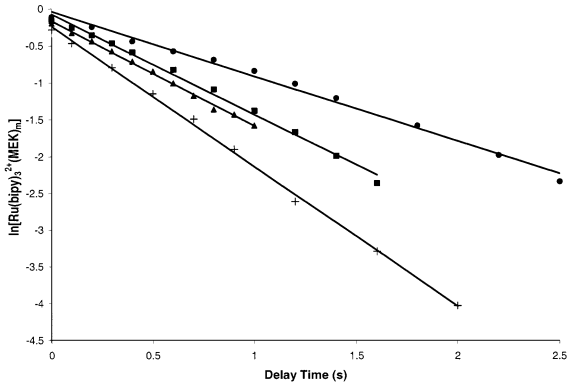

Figure 4. Solvent loss from $[Ru(bpy)_3]^{2+}(MEK)_m$ ($m = 1-4$) vs ion trapping time at 329 K and a pressure of 3×10^{-9} mbar. As the number of solvent molecules around the ruthenium complex ion increases, desolvation becomes a faster process. (●) $m = 1$, $k = 0.88 \pm 0.06$ s^{-1}; (■) $m = 2$, $k = 1.36 \pm 0.08$ s^{-1}; (▲) $m = 3$, $k = 1.42 \pm 0.06$ s^{-1}; (+) $m = 4$, $k = 1.90 \pm 0.07$ s^{-1}.

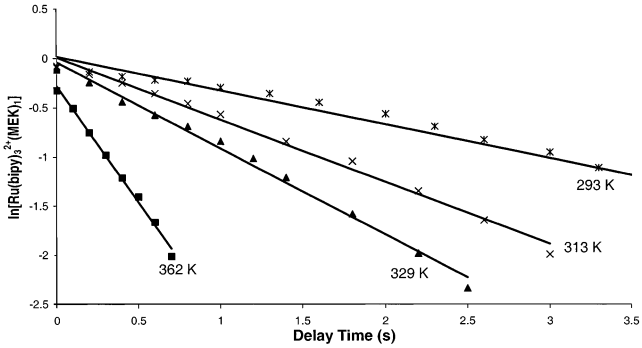

Figure 5. Loss of one MEK solvent molecule from $[Ru(bpy)_3]^{2+}(MEK)_1$ vs ion trapping time at several temperatures. $k(293\text{ K}) = 0.28 \pm 0.03$ s^{-1}, $k(313\text{ K}) = 0.63 \pm 0.04$ s^{-1}, $k(329\text{K}) = 0.88 \pm 0.06$ s^{-1}, $k(362\text{ K}) = 2.36 \pm 0.17$ s^{-1}.

Plots were also obtained for the dissociation of $[Ru(bpy)_3]^{2+}(MEK)_m$ at different temperatures within the range 294−365K. Figure 5 shows the loss of one MEK solvent molecule from $[Ru(bpy)_3]^{2+}(MEK)_1$ as a function of trapping time at several temperatures. Upon extraction of the rate constants from the slope of the lines in plots such as those shown in Figure 5, an Arrhenius plot such as the one shown in Figure 6 was generated. Zero-pressure experimental activation energies were then calculated by using the simple expression

$$E_a = -(Rm) \tag{9}$$

where R is the gas constant value and m is the slope of the line. The activation energies and preexponential factors obtained are summarized for $[Ru(bpy)_3]^{2+}(MEK)_m$ ($m = 1-4$) in Table 2. As the degree of solvation increases, there is a small decrease in activation energy for the dissociation of MEK from the ruthenium complex ion. Optimized structures obtained from ZINDO calculations (Figure 7) show that the carbonyl group

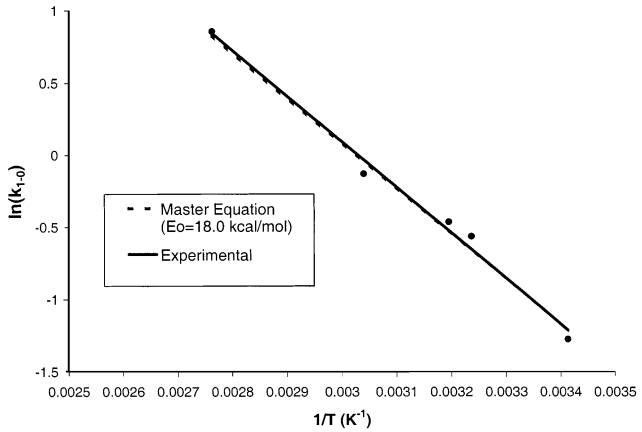

Figure 6. Temperature dependence plots (of $\ln(k_{1-0})$ vs $1/T$) for the loss of MEK solvent from $[Ru(bpy)_3]^{2+}(MEK)_1$. The dashed line represents the master equation fit to the experimental temperature dependence when $E_0 = 18.0$ kcal/mol.

from MEK binds with the hydrogens of the bipyridine ring. After four MEK molecules bind to $[Ru(bpy)_3]^{2+}$, a fifth solvent molecule would be expected to be more weakly bound. However, because the solvation range studied in the work reported here corresponds to only the first solvation shell, there should be no significant change in energy observed. Future studies will investigate the effect of greater solvation numbers on the dissociation energetics of these solvated ruthenium complex ions.

Pressure Dependence. As stated earlier, dissociation induced by BIRD should show unimolecular rate constants that are independent of pressure within the low-pressure regime. Additionally, the rate constant should have a nonzero value when extrapolated to zero pressure.[29] This type of behavior is observed for the solvated ruthenium complex ions whose dissociation is reported here. The rate constants as a function of background cell pressure shown in Figure 8 were obtained by monitoring the dissociation of $[Ru(bpy)_3]^{2+}(MEK)_1$ after ejection of all other ions from the ICR cell. Although there is a slight increase in the rate constant values as pressure increases, a 30-fold change between the lowest and highest pressures would be expected if collisional activation were the only mechanism for dissociation. Given the uncertainties in rate constant and pressure measurement and the behavior seen in Figure 8, we have assumed that the dissociation rate constants obtained at base analyzer pressure (ca. 2×10^{-9} mbar) reflect the zero pressure dissociation rate constant values. We conclude that a radiation-driven process provides the primary activation for the dissociation of $[Ru(bpy)_3]^{2+}$ solvated with MEK at the pressures used in this study.

Tris(2,2′-bipyridine)ruthenium(II) Solvated with Acetone and Acetonitrile. The change in rate constant observed for the dissociation of $[Ru(bpy)_3]^{2+}(acetone)_m$ and $[Ru(bpy)_3]^{2+}(ACN)_m$ is generally lower relative to that of $[Ru(bpy)_3]^{2+}(MEK)_m$ upon an increase in temperature. For this reason, the activation energy for loss of solvent molecule from $[Ru(bpy)_3]^{2+}(acetone)_m$ and $[Ru(bpy)_3]^{2+}(ACN)_m$ is less than that for the loss of solvent molecule from $[Ru(bpy)_3]^{2+}(MEK)_m$. Parts a and b of Figure 9 are kinetic plots for the dissociation of $[Ru(bpy)_3]^{2+}(acetone)_1$ and $[Ru(bpy)_3]^{2+}(ACN)_1$ to form the parent ruthenium complex ion at several temperatures.

The results from the Arrhenius plots show that the zero-pressure activation energies (also given in Table 2) for the dissociation of the solvent molecule from $[Ru(bpy)_3]^{2+}(acetone)_1$ and $[Ru(bpy)_3]^{2+}(ACN)_1$ are 4.5 ± 0.7 and 5.4 ± 0.8 kcal/mol, respectively. These results are 1−2 kcal/mol lower in energy than the E_a of $[Ru(bpy)_3]^{2+}(MEK)_1$. Given estimated errors for the E_a values, however, all values in Table 2 are essentially identical.

Truncated Boltzmann Calculations. The truncated Boltzmann approach has proven to be a useful one for calculating dissociation energies for a number of small-molecule cases.[27,31,49] However, for larger systems, this model has been shown to overestimate these bond dissociation energies.[32] The kinetic shift ($E_0 \neq E_t$) becomes more important following the transition from small to large-molecule behavior. To assess the accuracy of the truncated Boltzmann model when applied to the solvated ruthenium(II) complexes studied in this work, we obtained dissociation energies using it before proceeding to full master equation calculations. The Boltzmann distribution of ion internal energies for $[Ru(bpy)_3]^{2+}(MEK)_n$ ($m = 1-4$) using vibrational frequencies from ZINDO was calculated by using

$$P(E)\,\mathrm{d}E = \frac{W(E)\mathrm{e}^{-E/kT}\,\mathrm{d}E}{\int W(\epsilon)\,\mathrm{e}^{-E/kT}\,\mathrm{d}\epsilon} \qquad (10)$$

where $W(E)$ is the density of states at energy E, k is the Boltzmann constant, and T is the temperature. As the number of oscillators increases, the Boltzmann distribution of ion internal energies shifts to higher energy values.

The Boltzmann curve was truncated sharply at $E_t - {}^1/_2 h\nu_{av}$[27] to allow for reactive depletion of the ion population above threshold as well as the ion population that dissociates upon absorption of an "average" blackbody photon of energy $h\nu_{av}$. The value of the average blackbody photon energy was calculated by integrating under the blackbody curve at the average of the temperature range used in these experiments (at 330 K this value is approximately 1380 cm^{-1}). An initial value of E_t was chosen, and a subsequent value for the average truncated energy $\langle E' \rangle$ was calculated. The values were then input into eq 2 and compared to the experimentally determined activation energy. This cycle was repeated until an E_t value was chosen that would generate a value from the modified Tolman expression comparable with E_a (within 100 cm^{-1}). The results from the truncated Boltzmann approach are shown in Table 2 for $[Ru(bpy)_3]^{2+}(solvent)_1$ and for $[Ru(bpy)_3]^{2+}(MEK)_2$.

The values calculated from the truncated Boltzmann approach are substantially larger ($E_t \approx (3.5-4)E_a$) than the experimental activation energies. Given this large shift, a full master equation approach including RRKM (or PST) microcanonical rate constant calculations was next applied.

Master Equation Modeling. Results from ME modeling using the two different computational approaches described previously in the Computational Section are reported in Table 2. As would be expected, given the identical theoretical bases for these calculations, there is excellent agreement between the E_0 values obtained using the two different computational schemes at CWRU and at Marshall. The RRKM results from CWRU are generally slightly higher (of the order of 1 kcal/mol) than those from Marshall, which is attributable to the greater emphasis in the former case on the slopes as opposed to the absolute values of the rates. The PST results from CWRU are higher again by about 2 kcal/mol, which reflects the fact that the PST approach corresponds to an RRKM analysis using a limit of the loosest possible transition state. Thus these PST values correspond to the highest E_0 results that will be obtained by any transition-state parametrization within an RRKM-type analysis.

Considering the uncertainties in experimental data, in calculated infrared frequencies and transition dipoles, and in the

TABLE 2: Zero-Pressure Activation Energies, Truncated Boltzmann E_t Values, and E_0 Values Obtained from Master Equation (ME) Modeling for the Dissociation of $Ru(bpy)_3^{2+}(solvent)_1$ (All Energies in kcal/mol)

solvated complex ion	log A	E_a	E_t	E_0[a]	E_0[b]
$Ru(bpy)_3^{2+}(MEK)_1$	4.1 ± 0.8	6.3 ± 1.2	22.9 ± 1.3	18.0 (20.0)	17.6 ± 0.8
$Ru(bpy)_3^{2+}(MEK)_2$	3.4 ± 1.0	4.9 ± 1.2	21.3 ± 1.3	16.8 (18.5)	15.4 ± 0.7
$Ru(bpy)_3^{2+}(MEK)_3$	3.7 ± 0.8	5.3 ± 1.1		18.2 (20.5)	16.8 ± 0.8
$Ru(bpy)_3^{2+}(MEK)_4$	3.3 ± 0.3	4.5 ± 0.5		18.2 (21.7)	16.2 ± 1.0
$Ru(bpy)_3^{2+}(ACN)_1$	3.5 ± 0.5	5.4 ± 0.8	19.5 ± 0.9	17.1 (17.4)	17.3 ± 0.8
$Ru(bpy)_3^{2+}(acetone)_1$	3.0 ± 0.5	4.5 ± 0.7	16.4 ± 0.8	15.1 (16.2)	15.2 ± 0.9

[a] CWRU ME modeling, values in parentheses represent E_0 values obtained with PST-characterized transition states. [b] Marshall University ME modeling.

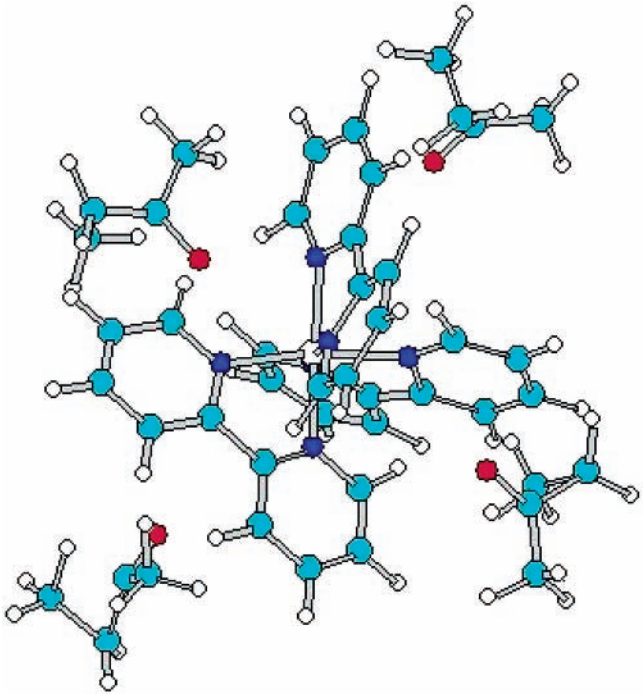

Figure 7. ZINDO optimized structure of $[Ru(bpy)_3]^{2+}$ $(MEK)_4$. The carbonyl oxygen is bridged between the hydrogens of the bipyridine rings.

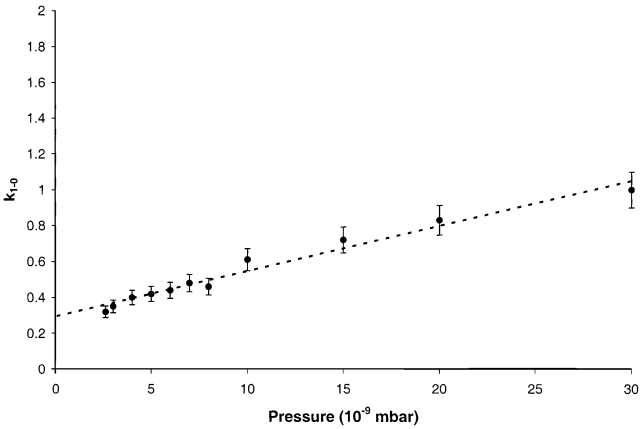

Figure 8. BIRD rate constant (k_{1-0}, <10% error) versus pressure for the loss of one MEK solvent from $[Ru(bpy)_3]^{2+}(MEK)_1$. $k(2.6 \times 10^{-9}$ mbar) = 0.32 s^{-1}, $k(3.0 \times 10^{-9}$ mbar) = 0.35 s^{-1}, $k(4.0 \times 10^{-9}$ mbar) = 0.40 s^{-1}, $k(5.0 \times 10^{-9}$ mbar) = 0.42 s^{-1}, $k(6.0 \times 10^{-9}$ mbar) = 0.44 s^{-1}, $k(7.0 \times 10^{-9}$ mbar) = 0.48 s^{-1}, $k(8.0 \times 10^{-9}$ mbar) = 0.46 s^{-1}, $k(10 \times 10^{-9}$ mbar) = 0.61 s^{-1}, $k(15 \times 10^{-9}$ mbar) = 0.72 s^{-1}, $k(20 \times 10^{-9}$ mbar) = 0.83 s^{-1}, and $k(30 \times 10^{-9}$ mbar) =1.0 s^{-1}.

correct frequencies to be used for transition states in PST or RRKM calculations of dissociation rates (as discussed in the Computational Section above), we believe a conservative

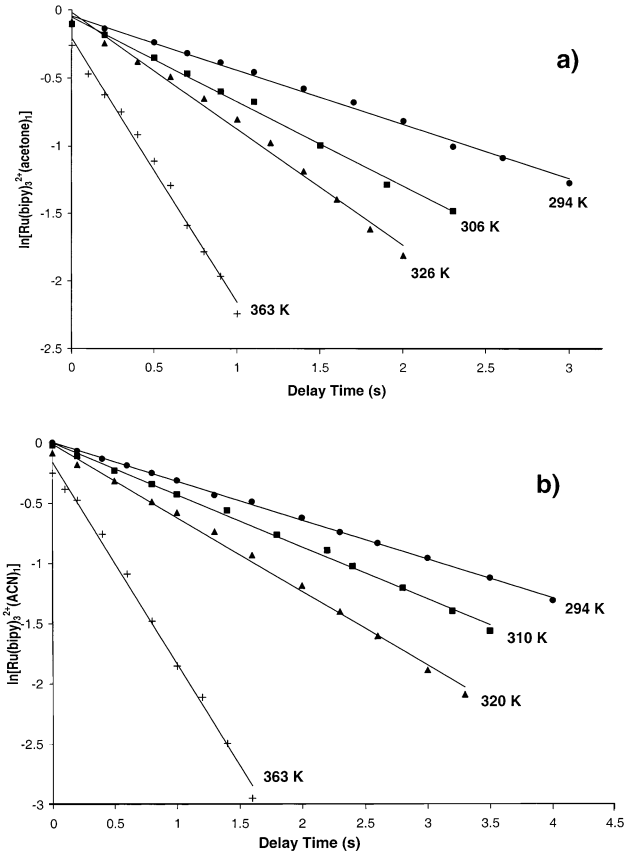

Figure 9. Dissociation temperature dependence for (a) $[Ru(bpy)_3]^{2+}$-$(acetone)_1$ [k(294 K) = 0.40 ± 0.02 s^{-1}, k(306 K) = 0.62 ± 0.04 s^{-1}, k(326 K) = 0.86 ± 0.06 s^{-1}, k(363 K) = 1.95 ± 0.13 s^{-1}] and (b) $[Ru(bpy)_3]^{2+}(ACN)_1$ [k(294 K) = 0.32 ± 0.01 s^{-1}, k(310 K) = 0.43 ± 0.02 s^{-1}, k(320 K) = 0.61 ± 0.03 s^{-1}, k(363K) = 1.80 ± 0.18 s^{-1}].

absolute error estimate of 3 kcal/mol should be given for the E_0 values obtained from ME modeling. Given the uncertainty dictated by this estimate, each of the six bond dissociation energies determined in this work can be assigned a value of 17.5 ± 3 kcal/mol. Comparisons of relative E_0 values within any one column in Table 2 can be made with more certainty, with estimated errors of ±1.0 kcal/mol. Thus the slightly lower E_0 value for $[Ru(bpy)_3]^{2+}(acetone)_1$ seen in each column may be significant. We also re-emphasize that ME-calculated E_0 values obtained for $[Ru(bpy)_3]^{2+}(acetonitrile)_1$ with scaled (by 0.95) vibrational frequencies calculated using DFT (17.6 kcal/mol) were virtually identical to E_0 values obtained with scaled (using eq 1) vibrational frequencies from ZINDO (17.1 kcal/mol as reported in Table 2).

To our knowledge, there has been no previous determination of gas-phase solvation energies for Ru(II) complexes such as those studied in this work. However, the E_0 values of ca. 17.5 kcal/mol reported here are quite consistent with those obtained

recently[25,50] for smaller ions (uncomplexed doubly charged alkaline ions) solvated by water. We would expect a major contribution to the solvation energy to be the ion−dipole interaction, where the potential energy is proportional to the dipole moment of the solvent molecule and inversely proportional to the square of the distance between the center of the dipole and the center of charge (assuming, to first order, that the 2+ charge on the Ru(II) complex ions is evenly distributed around the central ion and not polarized by the solvent dipole). In fact, the ion−dipole interaction energy calculated for a dipole moment of 3.0 D (the actual dipole moments of the solvents in this work are 3.92, 2.88, and 2.78 D for acetonitrile, acetone, and methyl ethyl ketone, respectively[51]) at a distance of 5.5 Å (average of maximum and "effective" thermodynamic radii of $[M(bpy)_3]^{2+}$ complexes[52]) from a 2+ ion is 14 kcal/mol.

Peschke et al.,[50] using high-pressure gas-phase equilibrium measurements, determined ΔH's of solvation, which decreased from 26 to 11 kcal/mol for the 6th through 14th water molecules surrounding dipositive alkaline earth ions. For these solvated ions, six water molecules form the first solvation shell, with the subsequent solvent molecules added to a second (or higher) shell. Values for the 7th and 8th water molecules for the various alkaline earth ions were found to be in the range 15−18 kcal/mol. Rodriguez-Cruz et al.[25] used the BIRD technique to study similar systems, and obtained E_0 values that decreased from 26 to 15 kcal/mol for the 5th through 7th solvating water molecule. The E_0's for the 7th water molecule ranged from 15 to 17 kcal/mol depending on the alkaline earth ion. The bpy ligands in the Ru(II) complexes studied in this work act as a first solvation shell around the central ion. Thus, the 1st through 4th solvents added would be similar to the 7th and subsequent water molecules added to the alkaline earth ions in the Peschke et al. and Rodriguez-Cruz et al. studies. Whereas the dipole moment of water (1.85 D)[51] is less than that of the three solvents used in this work, the effective radius of the first water solvation shell around the alkaline earth dipositive ions is expected to be less than the effective radius of the $[Ru(bpy)_3]^{2+}$ ions. Thus ion−dipole contributions to the solvation energies in the two systems should be similar, and the close agreement between values found in our study and the two recent ones[25,50] is quite reasonable. Additionally, the master equation E_0 values agree well with DFT-calculated binding energy values obtained in our labs for acetone (17.0 kcal/mol) and acetonitrile (15.2 kcal/mol) attached to the bipyridine ring of a smaller Ru(II) complex ion analogue $[Ru(NH_3)_4bpy]^{2+}$. Finally, inspection of Table 2 shows that the solvated ions studied in this work are sufficiently complex that E_t values obtained from the truncated Boltzmann approach do overestimate the true solvation energies, determined via master equation modeling. However, they are considerably closer to "true" values than activation energies obtained directly from Arrhenius plots.

Conclusions

Blackbody infrared radiative dissociation (BIRD) rate constants were determined for several of the solvent−complex dissociation pathways observed for tris(2,2′-bipyridine)ruthenium(II) complex ions solvated with methyl ethyl ketone, acetone, and acetonitrile. Pressure dependence studies show that BIRD is the most probable dissociation mechanism. Apparent activation energies for dissociation obtained from simple Arrhenius-type analyses are relatively low (4−7 kcal/mol). More detailed analyses provided by master equation calculations and the truncated Boltzmann approach indicate that the zero-pressure activation energies are substantially lower that the true bond dissociation energies. The bond dissociation energies, E_0, determined by ME calculations are all in the range 17.5 ± 3 kcal/mol. These values compare favorably with those obtained from DFT calculations in our laboratories and with recently reported values for the second solvation shell of doubly charged alkaline earth cations. Upon comparison with ab initio and experimental values, infrared intensities and scaled vibrational frequencies obtained from ZINDO computational methods were found to be suitable for master equation modeling. Future studies will examine Ru(II) complex ions surrounded by a larger number of solvent molecules, where a decrease in solvation energy should be seen as the solvents begin to occupy a second solvation shell.

Acknowledgment. This work was supported in part by the National Science Foundation (Grant No. CHE 97-27571).

References and Notes

(1) Gerardi, P. D.; Barnett, N. W.; Lewis, S. W. *Anal. Chim. Acta* **1999**, *378*, 1−41.
(2) Kalyanasundaram, K. *Coord. Chem. Rev.* **1982**, *46*, 159−244.
(3) (a) Meyer, T. J. *Prog. Inorg. Chem.* **1983**, *30*, 389. (b) Chang, Y. J.; Orman, L. K.; Anderson, D. R.; Yabe, T.; Hopkins, J. B. *J. Chem. Phys.* **1987**, *87*, 3249. (c) Juris, A.; Balzani, V.; Barigelletti, F.; Campagna, S.; Belser, P.; Vonselewsky, A. *Coord. Chem. Rev.* **1988**, *84*, 85−277. (d) Balzani, V.; Scandola, F. *Supramolecular Photochemistry*; Ellis Horwood: Chichester, U.K., 1991.
(4) Bradley, P. G.; Kress, N.; Hornberger, B. A.; Dallinger, R. F.; Woodruff, W. H. *J. Am. Chem. Soc.* **1981**, *103*, 1441.
(5) Strommen, D. P.; Mallick, P. K.; Danzer, G. D.; Lumpkin, R. S.; Kincaid, J. R. *J. Am. Chem. Soc.* **1990**, *94*, 1357.
(6) Ferguson, J.; Herren, F.; Krausz, E. R.; Maeder, M.; Vrbancich, J. *Coord. Chem. Rev.* **1985**, *64*, 21−39.
(7) Clark, C. D.; Hoffman, M. Z. *Coord. Chem. Rev.* **1997**, *159*, 359−373.
(8) Marshall, A. G.; Hendrickson, C. L.; Jackson, G. S. *Mass Spectrom. Rev.* **1998**, *17*, 1.
(9) Marshall, A. G. *Int. J. Mass Spectrom.* **2000**, *200*, 331.
(10) Bruce, J. E.; Anderson, G. A.; Wen, J.; Harkewicz, R.; Smith, R. D. *Anal. Chem.* **1999**, *71*, 2595.
(11) Marshall, A. G. *Adv. Mass Spectrom.* **1989**, *11A*, 651.
(12) Shi, S. H.; Hendrickson, C. L.; Marshall, A. G. *Proc. Natl. Acad. Sci. U.S.A.* **1998**, *95*, 11532.
(13) Dole, M.; Mack, L. L.; Hines, R. L.; Mobley, R. C.; Ferguson, L. D.; Alice, M. B. *J. Chem. Phys.* **1969**, *49*, 2240.
(14) Fenn, J. B.; Mann, M.: Meng, C. K.; Wong, S. F.; Whitehouse, C. M. *Science* **1989**, *246*, 64.
(15) Tholmann, D.; Tonner, D. S.; McMahon, T. B. *J. Phys. Chem.* **1994**, *98*, 2002.
(16) Price, W. D.; Schnier, P. D.; Williams, E. R. *Anal. Chem.* **1996**, *68*, 859.
(17) Gross, D. S.; Williams, E. R. *Int. J. Mass Spectrom. Ion Processes* **1996**, *158*, 305.
(18) Sena, M.; Riveros, J. M. *J. Phys. Chem. A* **1997**, *101*, 4384.
(19) Aaserud, D. J.; Guan, Z. Q.; Little, D. P.; McLafferty, F. W. *Int. J. Mass Spectrom.* **1997**, *167*, 705.
(20) Penn, S. G.; He, F.; Lebrilla, C. B. *J. Phys. Chem. B* **1998**, *102*, 9119.
(21) Jockusch, R. A.; Williams, E. R. *J. Phys. Chem. A* **1998**, *102*, 4543.
(22) Rodriguez-Cruz, S. E.; Jockusch, R. A.; Williams, E. R. *J. Am. Chem. Soc.* **1998**, *120*, 5842.
(23) Chen, O. N.; Groh, S.; Liechty, A.; Ridge, D. P. *J. Am. Chem. Soc.* **1999**, *121*, 11910.
(24) Butcher, D. J.; Asano, K. G.; Goeringer, D. E.; McLuckey, S. A. *J. Phys. Chem. A* **1999**, *103*, 8664.
(25) Rodriguez-Cruz, S. E.; Jockusch, R. A.; Williams, E. R. *J. Am. Chem. Soc.* **1999**, *121*, 8898.
(26) Strittmatter, E. F.; Wong, R. L.; Williams, E. R. *J. Phys. Chem. A* **2000**, *104*, 10271.
(27) Dunbar, R. C. *J. Phys. Chem.* **1994**, *98*, 8705.
(28) Price, W. D.; Williams, E. R. *J. Phys. Chem. A* **1997**, *101*, 8844.
(29) Dunbar, R. C.; McMahon, T. B. *Science* **1998**, *279*, 194.
(30) Dunbar, R. C.; Zaniewski, R. C. *J. Chem. Phys.* **1992**, *96*, 5069.
(31) Lin, C.-Y.; Dunbar, R. C. *J. Phys. Chem.* **1996**, *100*, 655.
(32) Price, W. D.; Schnier, P. D.; Williams, E. R. *J. Phys. Chem. B* **1997**, *101*, 664.
(33) Wigger, M.; Nawrocki, J. P.; Watson, C. H.; Eyler, J. R.; Benner, S. A. *Rapid Commun. Mass Spectrom.* **1997**, *11*, 1749.

(34) Spence, T. G.; Burns, T. D.; Posey, L. A. *J. Phys. Chem. A* **1997**, *101*, 139.
(35) De Koning, L. J.; Nibbering, N. M. M.; van Orden, S. L.; Laukien, F. H. *Int. J. Spectrom. Ion Processes* **1997**, *165/166*, 209.
(36) Ridley, J. E.; Zerner, M. C. *Theor. Chim. Acta* **1973**, 32, 111.
(37) Ridley, J. E.; Zerner, M. C. *Theor. Chim. Acta* **1976**, 42, 223.
(38) Lewis, N. A.; Pan, W.*Inorg. Chem*. **1995**, 34, 2244.
(39) Da Cunha, C. J.; Dodsworth, E. S.; Monteiro, M. A., Lever A. P. *Inorg. Chem*. **1999**, 38, 5399.
(40) Frisch, M. J.; Trucks, G. W.; Schlegel, H. B.; Scuseria, G. E.; Robb, M. A.; Cheeseman, J. R.; Zakrzewski, V. G.; Montgomery, J. A., Jr.; Stratmann, R. E.; Burant, J. C.; Dapprich, S.; Millam, J. M.; Daniels, A. D.; Kudin, K. N.; Strain, M. C.; Farkas, O.; Tomasi, J.; Barone, V.; Cossi, M.; Cammi, R.; Mennucci, B.; Pomelli, C.; Adamo, C.; Clifford, S.; Ochterski, J.; Petersson, G. A.; Ayala, P. Y.; Cui, Q.; Morokuma, K.; Malick, D. K.; Rabuck, A. D.; Raghavachari, K.; Foresman, J. B.; Cioslowski, J.; Ortiz, J. V.; Baboul, A. G.; Stefanov, B. B.; Liu, G.; Liashenko, A.; Piskorz, P.; Komaromi, I.; Gomperts, R.; Martin, R. L.; Fox, D. J.; Keith, T.; Al-Laham, M. A.; Peng, C. Y.; Nanayakkara, A.; Gonzalez, C.; Challacombe, M.; Gill, P. M. W.; Johnson, B. G.; Chen, W.; Wong, M. W.; Andres, J. L.; Head-Gordon, M.; Replogle, E. S.; Pople, J. A. *Gaussian 98*, revision A.7; Gaussian, Inc.: Pittsburgh, PA, 1998.
(41) Hay, P. J.; Wadt, W. R. *J. Chem. Phys.* **1985**, *82*, 270.
(42) Wadt, W. R.; Hay, P. J. *J. Chem. Phys.* **1985**, *82*, 284.
(43) Hay, P. J. *J. Chem. Phys.* **1985**, *82*, 299.
(44) Dunning, T. H., Jr.; Hay, P. J. In *Modern Theoretical Chemistry*; Schaefer, H. F., III, Ed.; Plenum: New York, 1976; pp 1−28.
(45) Beyer, T.; Swinehart, D. R. *ACM Commun.* **1973**, *16*, 379.
(46) Brown, P. N.; Byrne, G. D.; Hindmarsh, A. C. *SIAM J. Sci. Stat. Comput*. **1989**, *10*, 1038−1051.
(47) Klippenstein, S. J.; Wagner, A. F.; Dunbar, R. C.; Wardlaw, D. M.; Robertson, S. H.; Diau, E. W. VariFlex computer code, available at http://chemistry.anl.gov/chem-dyn/VariFlex/.
(48) Lifshitz, C. *Adv. Mass Spectrom.* **1989**, *11*, 113.
(49) Dunbar, R. C.; McMahon, T. B.; Thölmann, D.; Tonner, D. S.; Salahub, D. R.; Wei, D. *J. Am. Chem. Soc.* **1995**, *117*, 12819.
(50) Peschke, M.; Blades, A. T.; Kebarle, P. *J. Phys. Chem. A* **1998**, *102*, 9978.
(51) Lide, *D. R. Handbook of Chemistry and Physics*, 71st Ed.; CRC Press: Boca Raton, FL, 1990; **9**-6.
(52) Richardson, D. E. *Inorg. Chem.* **1990**, *29*, 3213.
(53) Mallick, P. K.; Danzer, G. D.; Strommen, D. P.; Kincaid, J. R. *J. Phys. Chem.* **1988**, *92*, 5628.